OPEN ACCESS Freely available online

PLOS ONE

Development of Novel Radiogallium-Labeled Bone Imaging Agents Using Oligo-Aspartic Acid Peptides as Carriers

Kazuma Ogawa[1]*, Atsushi Ishizaki[1], Kenichiro Takai[1], Yoji Kitamura[2], Tatsuto Kiwada[1], Kazuhiro Shiba[2], Akira Odani[1]

1 Graduate School of Medical Sciences, Kanazawa University, Kanazawa, Japan, **2** Advanced Science Research Center, Kanazawa University, Kanazawa, Japan

Abstract

^{68}Ga ($T_{1/2}$ = 68 min, a generator-produced nuclide) has great potential as a radionuclide for clinical positron emission tomography (PET). Because poly-glutamic and poly-aspartic acids have high affinity for hydroxyapatite, to develop new bone targeting ^{68}Ga-labeled bone imaging agents for PET, we used 1,4,7,10-tetraazacyclododecane-1,4,7,10-tetraacetic acid (DOTA) as a chelating site and conjugated aspartic acid peptides of varying lengths. Subsequently, we compared Ga complexes, Ga-DOTA-(Asp)$_n$ (n = 2, 5, 8, 11, or 14) with easy-to-handle ^{67}Ga, with the previously described ^{67}Ga-DOTA complex conjugated bisphosphonate, ^{67}Ga-DOTA-Bn-SCN-HBP. After synthesizing DOTA-(Asp)$_n$ by a Fmoc-based solid-phase method, complexes were formed with ^{67}Ga, resulting in ^{67}Ga-DOTA-(Asp)$_n$ with a radiochemical purity of over 95% after HPLC purification. In hydroxyapatite binding assays, the binding rate of ^{67}Ga-DOTA-(Asp)$_n$ increased with the increase in the length of the conjugated aspartate peptide. Moreover, in biodistribution experiments, ^{67}Ga-DOTA-(Asp)$_8$, ^{67}Ga-DOTA-(Asp)$_{11}$, and ^{67}Ga-DOTA-(Asp)$_{14}$ showed high accumulation in bone (10.5±1.5, 15.1±2.6, and 12.8±1.7% ID/g, respectively) but were barely observed in other tissues at 60 min after injection. Although bone accumulation of ^{67}Ga-DOTA-(Asp)$_n$ was lower than that of ^{67}Ga-DOTA-Bn-SCN-HBP, blood clearance of ^{67}Ga-DOTA-(Asp)$_n$ was more rapid. Accordingly, the bone/blood ratios of ^{67}Ga-DOTA-(Asp)$_{11}$ and ^{67}Ga-DOTA-(Asp)$_{14}$ were comparable with those of ^{67}Ga-DOTA-Bn-SCN-HBP. In conclusion, these data provide useful insights into the drug design of ^{68}Ga-PET tracers for the diagnosis of bone disorders, such as bone metastases.

Citation: Ogawa K, Ishizaki A, Takai K, Kitamura Y, Kiwada T, et al. (2013) Development of Novel Radiogallium-Labeled Bone Imaging Agents Using Oligo-Aspartic Acid Peptides as Carriers. PLoS ONE 8(12): e84335. doi:10.1371/journal.pone.0084335

Editor: Maxim Antopolsky, University of Helsinki, Finland

Received August 13, 2013; **Accepted** November 14, 2013; **Published** December 31, 2013

Funding: This work was supported in part by Grants-in-Aid for Young Scientists (B) (KAKENHI Grant Number 21791174 and 23791401) from the Ministry of Education, Culture, Sports, Science and Technology of Japan, Terumo Life Science Foundation, and Mochida Memorial Foundation for Medical and Pharmaceutical Research. The funders had no role in study design, data collection and analysis, decision to publish, or preparation of the manuscript.

Competing Interests: The authors have declared that no competing interests exist.

* E-mail: kogawa@p.kanazawa-u.ac.jp

Introduction

Bone contains abundant proliferation factors, and is therefore a convenient environment for tumors to metastasize and grow. Indeed, malignant tumors frequently metastasize to the bone [1]. With the development of therapeutic methods and drugs, early diagnoses of bone metastases must be more important. Significant advances in imaging technologies such as X-ray computed tomography (CT) and magnetic resonance imaging (MRI) have been made during the last a few decades; however, because of its high sensitivity, nuclear medicine bone scanning is the optimal test for detecting bone metastases. Over the last thirty years, ^{99m}Tc-bisphosphonate complexes such as methylenediphosphonate (^{99m}Tc-MDP) and hydroxymethylenediphosphonate (^{99m}Tc-HMDP) have been widely used as radiopharmaceuticals in bone scintigraphy for disorders such as metastatic bone cancer, Paget's disease, and osteoporotic fractures [2–5]. The accumulation of ^{99m}Tc-bisphoshonate complexes in bone must be derived from the binding of phosphonate groups in bisphosphonate to calcium (Ca^{2+}) in hydroxyapatite crystals in bone, but the mechanism of high uptake to lesion sites has not been completely elucidated. One of factors should be the increased vascularity and regional blood flow caused from disease. However, it has been reported that regional bone blood flow alone does not account for the increased uptake of ^{99m}Tc-bisphoshonate complexes [6]. Other factors should be involved in their binding and interaction with bone. It is generally assumed that ^{99m}Tc-bisphoshonate complexes accumulate at sites of active bone metabolism, especially, at osteoblastic lesions [7,8]. Newly formed bone has a much larger surface area than stable bone does. That is, the crystalline structure of hydroxyapatite in newly formed bone is amorphous and has a greater surface area than that in normal bone [9]. In the cases of ^{99m}Tc-bisphoshonate complexes, the phosphonate groups coordinate with not only Ca^{2+} but also ^{99m}Tc [10], which might decrease the inherent accumulation of bisphosphonate (MDP or HMDP) in bone. Incidentally, ^{99m}Tc-bisphoshonate complexes cannot be isolated as well-defined single chemical species, but as mixtures of short- and long-chain oligomers, may reduce the efficacy of radiopharmaceuticals. Biological behaviors of these tracers are also affected by the degree of ionization and by variable oligomer constitutions of preparations [11]. To overcome the shortcomings of ^{99m}Tc-bisphoshonate complexes, we and other groups have designed and developed ^{99m}Tc-mononuclear complex-conjugated

bisphosphonate compounds [12–15], in which phosphonate groups are not coordinated with ^{99m}Tc. As expected, some of these compounds showed superior biodistribution compared with previous compounds. Of note, this drug concept is applicable to both ^{99m}Tc-complex radiopharmaceuticals and other radiometals [16–26].

Sodium fluoride labeled with ^{18}F (^{18}F-NaF) for bone imaging was initially reported by Blau et al. in 1962 [27], and subsequently was approved by FDA in 1972. ^{18}F-NaF accumulates in bone because fluoride anions are isomorphously exchanged with the hydroxyl group in hydroxyapatite ($Ca_{10}(PO_4)_6(OH)_2$) and fluoroapatite ($Ca_{10}(PO_4)_6F_2$) is formed. After the development of ^{99m}Tc-labeled bone scintigraphy agents, such as ^{99m}Tc-MDP, ^{18}F-NaF was replaced by them because the physical characteristics of ^{99m}Tc were more convenient for imaging with conventional gamma cameras in those days. However, in the last two decades, positron emission tomography (PET) and PET/CT have evolved significantly and become widespread. The changes caused the reemergence of ^{18}F-NaF and bone imaging agents for PET are desired because current PET have higher spatial resolution and greater sensitivity than conventional gamma cameras. Actually, it was reported that ^{18}F-NaF PET imaging was significantly more sensitive than ^{99m}Tc-MDP planar and ^{99m}Tc-MDP single photon emission computed tomography (SPECT) imaging [28]. However, most positron emitters, such as ^{18}F, need high cost cyclotron facilities, and it limits the availability for PET.

Meanwhile, the radionuclide ^{68}Ga has great potential for clinical PET and could become an attractive alternative to ^{18}F because of its radiophysical properties, particularly as a generator-produced nuclide with a half-life ($T_{1/2}$) of 68 min [29]. Namely, it does not require an on-site cyclotron and can be eluted on demand. Indeed, in principle, the long half-life of the parent nuclide ^{68}Ge ($T_{1/2}$ = 270.8 days) provides a generator with a long life span. Therefore, the appearance of ^{68}Ga-labeled compounds for bone imaging has been desired and some compounds have been reported in recent years [30–34].

Several noncollagenous bone proteins have repeating sequences of acidic amino acids (Asp or Glu) in their structures, offering potential hydroxyapatite-binding sites. For example, osteopontin and bone sialoprotein, 2 major noncollagenous bone matrix proteins, have repeating Asp and Glu rich sequences, respectively [35–37]. Reportedly, poly-glutamic and poly-aspartic acids have high affinity for hydroxyapatite and could be used to deliver drugs to bone tissues [38–40].

In this study, to develop new PET tracers for imaging bone disorders such as bone metastases, because it is well known that ^{68}Ga forms a stable complex with 1,4,7,10-tetraazacyclododecane-1,4,7,10-tetraacetic acid (DOTA), DOTA was chosen as chelating sites. Subsequently, a series of Ga-DOTA-conjugated acidic amino acid peptides (Ga-DOTA-$(Asp)_n$; Figure 1A) of varying peptide lengths (n = 2, 5, 8, 11, or 14) were designed using the easy-to-handle radioisotope ^{67}Ga, and these were evaluated and compared, *in vitro* and *in vivo*, with the previously developed conjugated bisphosphonate complex ^{67}Ga-DOTA-Bn-SCN-HBP (Figure 1B) [33].

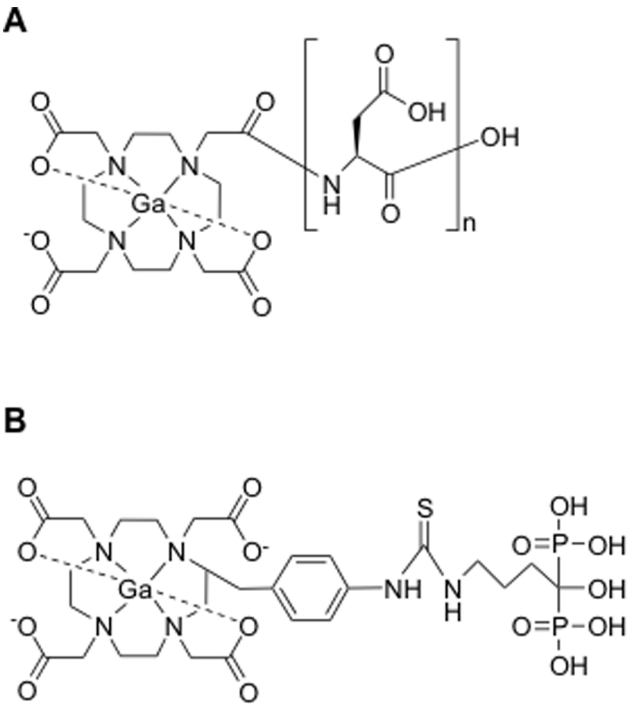

Figure 1. Structures. Chemical structures of (A) Ga-DOTA-$(Asp)_n$ (n = 2, 5, 8, 11, or 14) and (B) Ga-DOTA-Bn-SCN-HBP.
doi:10.1371/journal.pone.0084335.g001

Materials and Methods

Materials

Electrospray ionization mass spectra (ESI-MS) were obtained with a LCQ (Thermo Fisher Scientific, Waltham, MA, USA). Matrix assisted laser desorption/ionization-time of flight mass spectra (MALDI-TOF-MS) were obtained with ABI 4800 plus (AB SCIEX, Foster, CA, USA). [^{67}Ga]$GaCl_3$ was supplied by Nihon Medi-Physics Co., Ltd. (Tokyo, Japan). 1,4,7,10-Tetraazacyclododecane-1,4,7-tris(t-butyl acetate) (DOTA-tris) was purchased from Macrocyclics (Dallas, TX, USA). 9-Fluorenylmethoxycarbonyl (Fmoc)-Asp(OtBu)-Wang resin and Fmoc-Asp(OtBu) were purchased from Merck KGaA (Darmstadt, Germany). Alendronate was synthesized according to the previous reported method [18]. Other reagents were of reagent grade and used as received.

Synthesis of DOTA-$(Asp)_n$

The protected peptidyl resin was manually constructed by an Fmoc-based solid-phase methodology using Fmoc-Asp(OtBu)-Wang resin and Fmoc-Asp(OtBu). The peptide chain was constructed in cycles of (I) 15 minutes of deprotection with 20% piperidine in dimethylformamide (DMF) and (II) 2 hours of coupling with 3 equivalents of Fmoc-Asp(OtBu), 1,3-diisopropylcarbodiimide (DIPCDI) and 1-hydroxybenzotriazole hydrate (HOBt) in DMF. The coupling reaction was then repeated after Kaiser test was positive for the resin [41]. After construction of the peptide chain on the resin, the Fmoc protecting group was removed using 20% piperidine in DMF, and a mixture containing 2 equivalents of DOTA-tris, DIPCDI, and HOBt in DMF was added and allowed to react for 2 hours, as described above. To cleave peptides from the resin and deprotect, 0.5 mL of thioanisole and 5 mL of trifluoroacetic acid (TFA) were added to the fully protected peptide resin at 0°C and stirred at room temperature for 2 hours. After resin removal by filtration, ether was added to the filtrate at 0°C to precipitate crude peptide. The crude products were purified by reversed-phase (RP)-HPLC performed with a Hydrosphere 5C18 column (10×150 mm; YMC, Kyoto, Japan) at a flow rate of 4 mL/min with an isocratic mobile phase of water containing 0.1% TFA [in the case of DOTA-$(Asp)_2$] or with a Cosmosil 5C_{18}-AR 300 column (10×150 mm; Nacalai Tesque, Kyoto, Japan) at a flow rate of 4 mL/min with a 0–20% methanol

gradient mobile phase of 0.1% TFA in water over 20 minutes [in the case of DOTA-$(Asp)_n$ (n = 5, 8, 11, or 14)], respectively. Chromatograms were obtained by monitoring the UV adsorption at a wavelength of 220 nm. The fraction containing DOTA-$(Asp)_n$ (n = 2, 5, 8, 11, or 14) was determined by mass spectrometry, and collected. The solvent was removed by lyophilization to provide DOTA-$(Asp)_n$ as white powder.

DOTA-$(Asp)_2$ MS (ESI): m/z 635 $(M+H)^+$, Yield : 22.0%
DOTA-$(Asp)_5$ MS (ESI): m/z 980 $(M+H)^+$, Yield : 18.6%
DOTA-$(Asp)_8$ MS (ESI): m/z 1325 $(M+H)^+$, Yield : 36.0%
DOTA-$(Asp)_{11}$ MS (ESI): m/z 1670 $(M+H)^+$, Yield : 20.2%
DOTA-$(Asp)_{14}$ MS (MALDI): m/z 2015 $(M+H)^+$, Yield : 5.0%

Preparation of Ga-DOTA-$(Asp)_n$ (n = 2, 5, 8, 11, or 14)

DOTA-$(Asp)_n$ (n = 2, 5, 8, 11, or 14) (1 μmol) was dissolved in 75 μL of water, and $Ga(NO_3)_3$ (0.77 mg, 3 μmol) was added to the DOTA-$(Asp)_n$ solution. The mixture was reacted at 40°C for 2 hours. Ga-DOTA-$(Asp)_n$ was purified by RP-HPLC performed with a Hydrosphere 5C18 column (4.6×250 mm; YMC) at a flow rate of 1 mL/min with an isocratic mobile phase of water containing 0.1% TFA [in the case of Ga-DOTA-$(Asp)_2$] or with a Cosmosil $5C_{18}$-AR 300 column (4.6×150 mm) at a flow rate of 1 mL/min with a 0–20% methanol gradient mobile phase of 0.1% TFA in water over 20 minutes [in the case of DOTA-$(Asp)_n$ (n = 5, 8, 11, or 14)]. Chromatograms were obtained by monitoring the UV adsorption at a wavelength of 220 nm. The fraction containing DOTA-$(Asp)_n$ (n = 2, 5, 8, 11, or 14) was determined by mass spectrometry, and collected.

Ga-DOTA-$(Asp)_2$ MS (ESI): m/z 701 $(M+H)^+$
Ga-DOTA-$(Asp)_5$ MS (ESI): m/z 1046 $(M+H)^+$
Ga-DOTA-$(Asp)_8$ MS (ESI): m/z 1391 $(M+H)^+$
Ga-DOTA-$(Asp)_{11}$ MS (ESI): m/z 1736 $(M+H)^+$
Ga-DOTA-$(Asp)_{14}$ MS (MALDI): m/z 2081 $(M+H)^+$

Preparation of ^{67}Ga-DOTA-$(Asp)_n$ (n = 2, 5, 8, 11, or 14)

Approximately 50 μg of DOTA-$(Asp)_n$ (n = 2, 5, 8, 11, or 14) conjugates were dissolved in 75 μL of 0.2 M ammonium acetate buffer (pH 5.0), and 25 μL of $^{67}GaCl_3$ solution (1.85 MBq) in 0.01 M HCl was added and allowed to react at 80°C for 8 minutes. ^{67}Ga-DOTA-$(Asp)_n$ was purified by RP-HPLC under the conditions described for Ga-DOTA-$(Asp)_n$.

Hydroxyapatite-binding Assays

Hydroxyapatite-binding assays were performed according to previously described procedures with slight modifications [33]. In brief, hydroxyapatite beads (Bio-Gel; Bio-Rad, Hercules, CA, USA) were suspended in Tris/HCl-buffered saline (50 mM, pH 7.4) at 2.5 mg/mL, 10 mg/mL, and 25 mg/mL. For the solutions of ^{67}Ga-DOTA-$(Asp)_n$ (n = 2, 5, 8, 11, or 14), the ligand concentrations were adjusted to 19.5 μM by adding DOTA-$(Asp)_n$. Two hundred microliters of each ^{67}Ga-DOTA-$(Asp)_n$ solution was added to 200 μL of the hydroxyapatite suspension, and the samples were gently shaken for 1 hour at room temperature. After centrifugation at 10,000 *g* for 5 minutes, the radioactivity of the supernatants was measured using an auto well gamma counter (ARC-7010B, Hitachi Aloka Medical, Ltd., Tokyo, Japan). Control experiments were performed using the same procedure without hydroxyapatite beads, which showed less than 0.1% adsorption of radioactivity to vials. The ratios of binding were determined as follows:

$$\text{Hydroxyapatite binding}(\%) = \left(\begin{array}{l}\text{1-[sample supernatant radioactivity]/}\\ \text{[control supernatant radioactivity]}\end{array}\right) \times 100$$

The effect of bisphosphonate on the binding of ^{67}Ga-DOTA-$(Asp)_{14}$ or ^{67}Ga-DOTA-Bn-SCN-HBP to hydroxyapatite beads was also examined. In these experiments, 100 μL of ^{67}Ga-DOTA-$(Asp)_{14}$ or ^{67}Ga-DOTA-Bn-SCN-HBP solutions containing varying concentrations of the bisphosphonate compound alendronate were incubated with 100 μL of suspensions containing 1 mg of hydroxyapatite beads. After centrifugation, the radioactivity of the supernatant was measured, and hydroxyapatite-binding ratios were calculated as described above.

Biodistribution Experiments

Experiments with animals were conducted in strict accordance with the Guidelines for the Care and Use of Laboratory Animals of Kanazawa University. The animal experimental protocols used were approved by the Committee on Animal Experimentation of Kanazawa University (Permit Number: AP-132633). Biodistribution experiments were performed after an intravenous administration of each diluted tracer solution (37 kBq/100 μL) to 6-week-old male ddY mice (27–32 g, Japan SLC, Inc., Hamamatsu, Japan). To investigate the effect of an excess amount of bisphosphonate on biodistribution, alendronate (20 mg/kg) was intravenously administered to mice 1 minute before the intravenous injection of ^{67}Ga-DOTA-$(Asp)_{14}$ or ^{67}Ga-DOTA-Bn-SCN-HBP. Four to six mice each were sacrificed by decapitation at 10, 60, and 180 minutes post-injection. Tissues of interest were removed and weighed. Complete left femurs were isolated as representative bone samples, radioactivity was determined using an auto well gamma counter, and counts were corrected for background radiation and physical decay during counting.

Protein-binding Assay

Serum protein binding ratios of ^{67}Ga-DOTA-$(Asp)_n$ (n = 2, 5, 8, 11, or 14) and ^{67}Ga-DOTA-Bn-SCN-HBP were evaluated by an ultrafiltration method. In these experiments, 6-week-old male ddY mice received intravenous boluses of radiotracer. After 3 minutes,

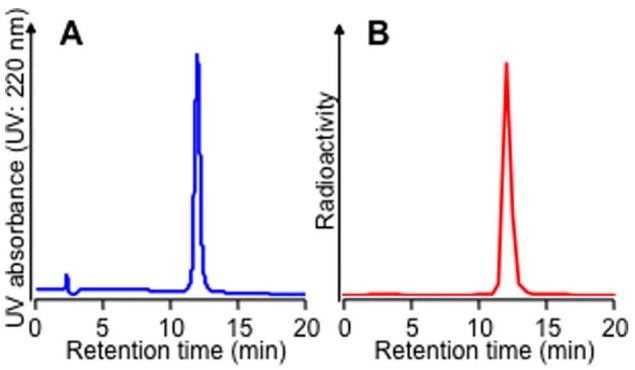

Figure 2. RP-HPLC chromatograms. RP-HPLC chromatograms of (A) nonradioactive Ga-DOTA-$(Asp)_{14}$ and (B) ^{67}Ga-DOTA-$(Asp)_{14}$. Conditions: A flow rate of 1 mL/min with a gradient mobile phase of 100% water containing 0.1% TFA to 20% methanol in water containing 0.1% TFA for 20 minutes.
doi:10.1371/journal.pone.0084335.g002

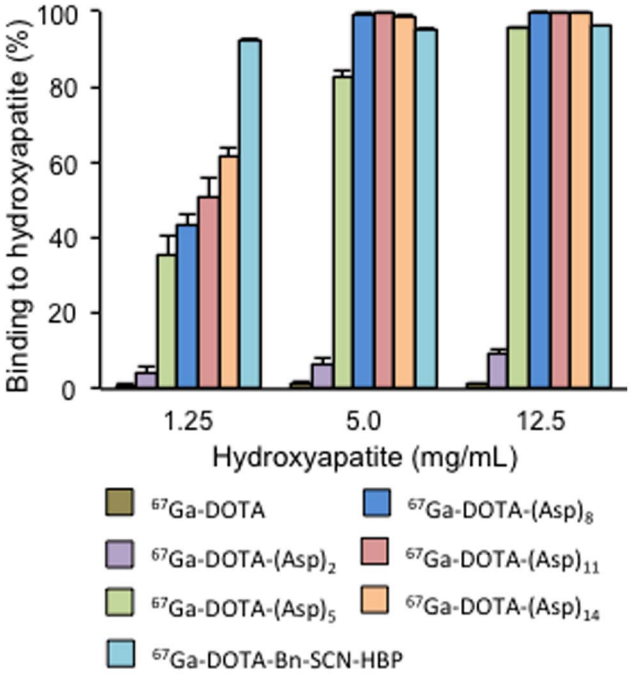

Figure 3. Hydroxyapatite binding assay. Binding ratios of ^{67}Ga-DOTA, ^{67}Ga-DOTA-(Asp)$_n$ (n = 2, 5, 8, 11, or 14), and ^{67}Ga-DOTA-Bn-SCN-HBP to hydroxyapatite beads. Data are expressed as the mean ± SD for four samples.
doi:10.1371/journal.pone.0084335.g003

the mice were anesthetized with ether, and blood was collected by heart puncture. Serum samples were prepared and applied to an Amicon Ultra-0.5 Centrifugal Filter Unit with Ultracel-30 membrane (Millipore). The units were centrifuged at 14,000 *g* for 20 minutes at room temperature. The radioactivity counts of the initials and filtrates were determined using an auto well gamma counter. The protein-binding ratios were then calculated as follows:

$$\text{Protein-binding ratio}(\%) = 100 - (\text{radioactivity of filtrate})/(\text{radioactivity of initial solution}) \times 100$$

Statistical Analysis

Data are expressed as means ± standard deviations where appropriate. In biodistribution experiments using alendronate as a blocking agent, differences were identified using unpaired Students' *t* test and were considered significant when $p<0.05$.

Results

Preparation of ^{67}Ga-DOTA-(Asp)$_n$ (n = 2, 5, 8, 11, or 14)

^{67}Ga-DOTA-(Asp)$_n$ (n = 2, 5, 8, 11, or 14) was prepared by complexation of DOTA-(Asp)$_n$ with ^{67}Ga. Radiochemical yields of ^{67}Ga-DOTA-(Asp)$_2$, ^{67}Ga-DOTA-(Asp)$_5$, ^{67}Ga-DOTA-(Asp)$_8$, ^{67}Ga-DOTA-(Asp)$_{11}$, and ^{67}Ga-DOTA-(Asp)$_{14}$, were 25%, 67%, 74%, 56%, and 51%, respectively. After RP-HPLC purification, ^{67}Ga-DOTA-(Asp)$_n$ had a radiochemical purity of over 95%. Figure 2 shows typical chromatograms of ^{67}Ga-DOTA-(Asp)$_{14}$ and Ga-DOTA-(Asp)$_{14}$. RP-HPLC analyses of ^{67}Ga-DOTA-(Asp)$_n$ and Ga-DOTA-(Asp)$_n$ showed similar retention times, indicating that the radiogallium-labeled product was identical to its authentic nonradioactive counterpart.

Hydroxyapatite-binding Assay

Figure 3 shows the percentage of each ^{67}Ga-DOTA-(Asp)$_n$ (n = 2, 5, 8, 11, or 14) that was bound to hydroxyapatite beads. Binding of each ^{67}Ga-DOTA-(Asp)$_n$ to hydroxyapatite beads increased with the amount of hydroxyapetite. In contrast, ^{67}Ga-DOTA and ^{67}Ga-DOTA-(Asp)$_2$ hardly bound to hydroxyapatite beads. Moreover, hydroxyapetite binding of ^{67}Ga-DOTA-(Asp)$_n$ increased with the increase in the length of the aspartic acid chain. On the other hand, the binding of ^{67}Ga-DOTA-(Asp)$_{14}$ and ^{67}Ga-DOTA-Bn-SCN-HBP was inhibited by the addition of a bisphosphonate compound alendronate in a concentration-dependent manner (Figure 4). Although ^{67}Ga-DOTA-Bn-SCN-HBP had higher affinity for hydroxyapatite than ^{67}Ga-DOTA-(Asp)$_{14}$ (Figure 3), ^{67}Ga-DOTA-Bn-SCN-HBP appeared more susceptible to alendronate inhibition than ^{67}Ga-DOTA-(Asp)$_{14}$ (Figure 4).

Biodistribution Experiments

The biodistributions of ^{67}Ga-DOTA-(Asp)$_n$ compounds (n = 2, 5, 8, 11, or 14) in normal mice are listed in Tables 1–5. Among these, ^{67}Ga-DOTA-(Asp)$_8$, ^{67}Ga-DOTA-(Asp)$_{11}$, and ^{67}Ga-DOTA-(Asp)$_{14}$ showed higher accumulation, and led to sustained radioactivity in the femur. Though ^{67}Ga-DOTA-(Asp)$_5$ led to moderate accumulation of radioactivity in the femur at 10 min after injection, the radioactivity was not retained. Meanwhile, ^{67}Ga-DOTA-(Asp)$_2$ hardly accumulated in the femur, and almost all injected radioactivity was rapidly excreted via the kidneys. Almost all radioactivity except radioactivity in bone after injection of ^{67}Ga-DOTA-(Asp)$_n$ compounds (n = 5, 8, 11, or 14) was also quickly excreted via the kidneys. Consequently, radioactivity was scarcely observed in any tissues except the bone and kidney at 60 minutes after injection of ^{67}Ga-DOTA-(Asp)$_n$ compounds (n = 5, 8, 11, or 14).

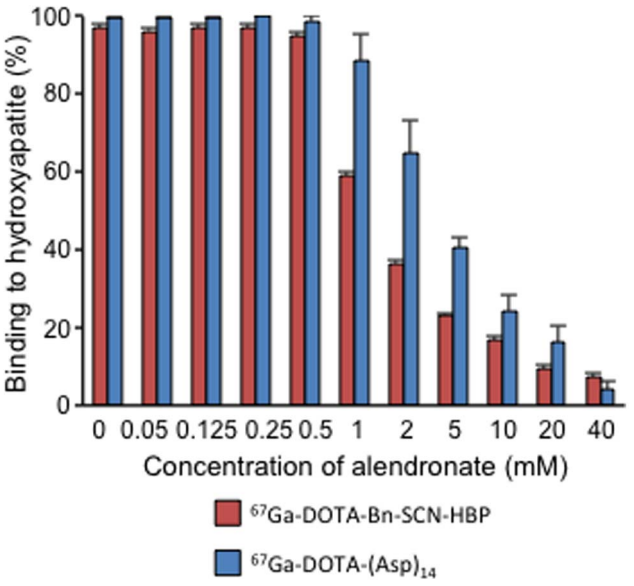

Figure 4. Inhibition using alendronate. Binding ratios of ^{67}Ga-DOTA-(Asp)$_{14}$ and ^{67}Ga-DOTA-Bn-SCN-HBP to hydroxyapatite in the presence of various concentrations of the inhibitor alendronate. Data are expressed as the mean ± SD for four samples.
doi:10.1371/journal.pone.0084335.g004

Table 1. Biodistribution of radioactivity after intravenous administration of ^{67}Ga-DOTA-$(Asp)_2$ in mice.[a]

	Time after administration		
Tissue	**10 min**	**60 min**	**180 min**
Blood	2.69 (0.42)	0.24 (0.08)	0.07 (0.06)
Liver	0.67 (0.11)	0.31 (0.28)	0.11 (0.02)
Kidney	11.77 (1.92)	8.87 (4.09)	1.31 (0.50)
Small-intestine	0.57 (0.08)	0.22 (0.12)	0.08 (0.03)
Large-intestine	0.46 (0.07)	0.07 (0.01)	0.40 (0.30)
Spleen	0.61 (0.01)	0.14 (0.04)	0.12 (0.02)
Pancreas	0.76 (0.14)	0.16 (0.05)	0.08 (0.03)
Lung	2.10 (0.22)	0.24 (0.06)	0.08 (0.02)
Heart	0.98 (0.15)	0.13 (0.05)	0.06 (0.04)
Stomach[b]	0.28 (0.05)	0.07 (0.04)	0.05 (0.04)
Bone (Femur)	1.48 (0.31)	0.80 (0.40)	0.38 (0.15)
Muscle	0.76 (0.28)	0.13 (0.05)	0.07 (0.02)
Brain	0.08 (0.02)	0.02 (0.01)	0.01 (0.01)
F/B ratio[c]	0.55 (0.07)	3.28 (1.23)	8.04 (4.50)

[a]Expressed as % injected dose. Each value represents the mean (SD) for five animals.
[b]Expressed as % injected dose.
[c]Femur:blood ratio.
doi:10.1371/journal.pone.0084335.t001

Table 2. Biodistribution of radioactivity after intravenous administration of ^{67}Ga-DOTA-$(Asp)_5$ in mice.[a]

	Time after administration		
Tissue	**10 min**	**60 min**	**180 min**
Blood	2.18 (0.13)	0.16 (0.04)	0.02 (0.01)
Liver	0.44 (0.07)	0.07 (0.01)	0.04 (0.01)
Kidney	8.42 (1.82)	3.61 (1.12)	0.91 (0.27)
Small-intestine	0.42 (0.06)	0.11 (0.04)	0.03 (0.01)
Large-intestine	0.37 (0.04)	0.19 (0.15)	0.07 (0.01)
Spleen	0.50 (0.04)	0.07 (0.02)	0.03 (0.00)
Pancreas	0.65 (0.07)	0.13 (0.07)	0.02 (0.00)
Lung	1.50 (0.13)	0.15 (0.04)	0.02 (0.01)
Heart	0.79 (0.08)	0.07 (0.02)	0.03 (0.01)
Stomach[b]	0.24 (0.03)	0.05 (0.02)	0.03 (0.01)
Bone (Femur)	6.36 (0.86)	3.63 (0.29)	1.76 (0.04)
Muscle	0.63 (0.21)	0.09 (0.05)	0.03 (0.01)
Brain	0.08 (0.02)	0.01 (0.00)	0.00 (0.00)
F/B ratio[c]	2.91 (0.34)	23.33 (4.84)	85.54 (26.61)

[a]Expressed as % injected dose. Each value represents the mean (SD) for four animals.
[b]Expressed as % injected dose.
[c]Femur:blood ratio.
doi:10.1371/journal.pone.0084335.t002

The biodistribution of ^{67}Ga-DOTA-$(Asp)_{14}$ after pretreatment of normal mice with alendronate (20 mg/kg) is presented in Table 6. Table 7 and reference 29 show biodistribution of ^{67}Ga-DOTA-Bn-SCN-HBP with or without pretreatment of alendronate (20 mg/kg). Although pretreatment with the same dose of alendronate significantly inhibited the accumulation of ^{67}Ga-DOTA-Bn-SCN-HBP in bone (17.44±1.12 and 8.59±0.81%ID/g at 10 min, 22.28±2.15 and 13.47±1.76%ID/g at 1 h, 23.53±2.34 and 13.30±2.10%ID/g at 3 h), alendronate had comparatively little effect on the bone accumulation of ^{67}Ga-DOTA-$(Asp)_{14}$.

Protein-binding Assay

Proportions of ^{67}Ga-DOTA-$(Asp)_n$ (n = 2, 5, 8, 11, or 14) and ^{67}Ga-DOTA-Bn-SCN-HBP bound to serum protein (Figure 5) shows that the binding of ^{67}Ga-DOTA-$(Asp)_n$ compounds to serum proteins decreased with an increase in the length of the aspartic acid chain. The serum protein binding rate of ^{67}Ga-DOTA-Bn-SCN-HBP was greater than that of ^{67}Ga-DOTA-$(Asp)_n$ compounds.

Discussion

Previously, we introduced the concept of radiometal complex-conjugated bisphosphonate compounds for the development of bone-seeking radiopharmaceuticals [42,43]. Moreover, in recent years, superior activities of newly developed radiogallium complex-conjugated bisphosphonate compounds have been reported by us and other groups [30–34]. In these drug compounds, the bisphosphonate structure has high affinity for hydroxyapatite, which is a specific component of bone tissues, leading to targeting of bone tissues. In a previous study, it was reported that the *in vitro* binding profile of Fmoc-$(Asp)_n$ (n = 2, 4, 6, 8, or 10) to hydroxyapatite increased with the increase in the length of the peptide [44]. Here a similar strategy was applied using aspartic acid peptides as the carrier to bone tissues instead of bisphosphonate. Indeed, we have demonstrated that the binding of ^{67}Ga-DOTA-$(Asp)_n$ (n = 5, 8, 11, or 14) to hydroxyapatite beads increased with increased length of the aspartic acid peptide. This

Table 3. Biodistribution of radioactivity after intravenous administration of ^{67}Ga-DOTA-$(Asp)_8$ in mice.[a]

	Time after administration		
Tissue	**10 min**	**60 min**	**180 min**
Blood	2.06 (0.18)	0.14 (0.07)	0.07 (0.01)
Liver	0.46 (0.06)	0.10 (0.08)	0.07 (0.01)
Kidney	9.88 (5.74)	2.60 (2.40)	1.20 (0.61)
Small-intestine	0.49 (0.05)	0.15 (0.10)	0.09 (0.03)
Large-intestine	0.39 (0.06)	0.05 (0.01)	0.17 (0.07)
Spleen	0.42 (0.09)	0.11 (0.15)	0.06 (0.01)
Pancreas	0.56 (0.14)	0.07 (0.04)	0.05 (0.02)
Lung	1.59 (0.16)	0.14 (0.05)	0.07 (0.02)
Heart	1.09 (0.44)	0.06 (0.02)	0.04 (0.03)
Stomach[b]	0.29 (0.16)	0.05 (0.05)	0.04 (0.03)
Bone (Femur)	11.65 (0.49)	12.56 (3.09)	11.29 (0.62)
Muscle	0.87 (0.51)	0.09 (0.06)	0.09 (0.07)
Brain	0.10 (0.04)	0.03 (0.02)	0.02 (0.02)
F/B ratio[c]	5.69 (0.42)	102.00 (41.75)	171.85 (26.47)

[a]Expressed as % injected dose. Each value represents the mean (SD) for five animals.
[b]Expressed as % injected dose.
[c]Femur:blood ratio.
doi:10.1371/journal.pone.0084335.t003

Table 4. Biodistribution of radioactivity after intravenous administration of ^{67}Ga-DOTA-(Asp)$_{11}$ in mice.[a]

	Time after administration		
Tissue	**10 min**	**60 min**	**180 min**
Blood	1.51 (0.16)	0.11 (0.02)	0.03 (0.01)
Liver	0.44 (0.12)	0.07 (0.01)	0.05 (0.01)
Kidney	16.04 (7.49)	1.76 (1.38)	0.80 (0.21)
Small-intestine	0.41 (0.04)	0.27 (0.37)	0.05 (0.02)
Large-intestine	0.27 (0.02)	0.06 (0.06)	0.13 (0.05)
Spleen	0.31 (0.08)	0.09 (0.06)	0.04(0.02)
Pancreas	0.62 (0.20)	0.07 (0.06)	0.05 (0.01)
Lung	1.11 (0.16)	0.12 (0.09)	0.04 (0.01)
Heart	0.55 (0.04)	0.08 (0.05)	0.02 (0.02)
Stomach[b]	0.21 (0.02)	0.18 (0.35)	0.04 (0.01)
Bone (Femur)	13.09 (1.16)	16.30 (3.58)	13.91 (1.93)
Muscle	0.48 (0.06)	0.13 (0.11)	0.08 (0.05)
Brain	0.05 (0.02)	0.02 (0.01)	0.01 (0.01)
F/B ratio[c]	8.71 (0.73)	156.07 (45.00)	501.32 (156.89)

[a]Expressed as % injected dose. Each value represents the mean (SD) for five animals.
[b]Expressed as % injected dose.
[c]Femur:blood ratio.
doi:10.1371/journal.pone.0084335.t004

Table 5. Biodistribution of radioactivity after intravenous administration of ^{67}Ga-DOTA-(Asp)$_{14}$ in mice.[a]

	Time after administration		
Tissue	**10 min**	**60 min**	**180 min**
Blood	1.61 (0.09)	0.07 (0.01)	0.03 (0.01)
Liver	0.39 (0.06)	0.05 (0.01)	0.05 (0.01)
Kidney	12.43 (5.81)	0.99 (0.17)	0.76 (0.10)
Small-intestine	0.38 (0.06)	0.08 (0.02)	0.05 (0.02)
Large-intestine	0.30 (0.04)	0.04 (0.01)	0.15 (0.08)
Spleen	0.42 (0.11)	0.07 (0.02)	0.03 (0.01)
Pancreas	0.50 (0.02)	0.07 (0.02)	0.03 (0.01)
Lung	1.19 (0.14)	0.08 (0.01)	0.03 (0.00)
Heart	0.62 (0.06)	0.06 (0.00)	0.03 (0.00)
Stomach[b]	0.24 (0.06)	0.10 (0.07)	0.02 (0.01)
Bone (Femur)	10.08 (0.86)	12.81 (1.67)	13.27 (1.15)
Muscle	0.57 (0.19)	0.08 (0.02)	0.05 (0.03)
Brain	0.05 (0.01)	0.01 (0.00)	0.01 (0.00)
F/B ratio[c]	6.27 (0.66)	185.54 (46.89)	591.08 (221.41)

[a]Expressed as % injected dose. Each value represents the mean (SD) for five animals.
[b]Expressed as % injected dose.
[c]Femur:blood ratio.
doi:10.1371/journal.pone.0084335.t005

result is consistent with the previous study and was reflected by bone accumulation of ^{67}Ga-DOTA-(Asp)$_n$ in biodistribution experiments. Moreover, these biodistribution experiments showed greater bone accumulation with increasing length of the peptide conjugates from ^{67}Ga-DOTA-(Asp)$_2$ to ^{67}Ga-DOTA-(Asp)$_{11}$. The longer compounds ^{67}Ga-DOTA-(Asp)$_{11}$ and ^{67}Ga-DOTA-(Asp)$_{14}$ accumulated equally in bone and showed superior biodistribution characteristics as that of bone imaging radiopharmaceuticals, with high accumulation in bone and rapid clearance from other tissues. Despite lower bone accumulation than the bisphosphonate ^{67}Ga-DOTA-Bz-SCN-HBP, the bone/blood ratios of radioactivity after injection of ^{67}Ga-DOTA-(Asp)$_{11}$ and ^{67}Ga-DOTA-(Asp)$_{14}$, which are an index as bone imaging, were comparable or higher (Figure 6), presumably due to more rapid blood clearance than ^{67}Ga-DOTA-Bz-SCN-HBP. This may reflect the lower serum protein binding ratios of ^{67}Ga-DOTA-(Asp)$_{11}$ and ^{67}Ga-DOTA-(Asp)$_{14}$ compared to that of ^{67}Ga-DOTA-Bn-SCN-HBP (Figure 5).

We assumed that the high accumulation of radioactivity in the bone after injection of these compounds was due to hydroxyapatite binding of bisphosphonate or aspartic acid structures in bone tissues. To estimate the hydroxyapatite binding of these compounds, alendronate inhibition experiments were performed *in vitro* and *in vivo*. In these hydroxyapatite binding assays, ^{67}Ga-DOTA-(Asp)$_{14}$ and ^{67}Ga-DOTA-Bn-SCN-HBP binding was inhibited by alendronate, confirming that the mechanism by which ^{67}Ga-DOTA-(Asp)$_{14}$ and ^{67}Ga-DOTA-Bn-SCN-HBP accumulate in bone involves coordination of their functional groups to the Ca^{2+} in hydroxyapatite crystals [45]. However, ^{67}Ga-DOTA-Bn-SCN-HBP binding was inhibited by lower concentrations of alendronate compared with ^{67}Ga-DOTA-(Asp)$_{14}$. Moreover, in biodistribution experiments, the inhibition of radioactive bone accumulation by alendronate was greater after injection of ^{67}Ga-DOTA-Bn-SCN-HBP than that of ^{67}Ga-DOTA-(Asp)$_{14}$. Although the precise mechanisms remain unclear, the binding patterns of these compounds to hydroxyapatite may differ. Wang *et al.* reported that alendronate and (D-Asp)$_8$, which were used as bone-targeting moieties on conjugated fluorescein isothiocyanate

Table 6. Biodistribution of radioactivity after intravenous administration of ^{67}Ga-DOTA-(Asp)$_{14}$ in mice with pretreatment of alendronate (20 mg/kg).[a]

	Time after administration		
Tissue	**10 min**	**60 min**	**180 min**
Blood	1.94 (0.33)	0.23 (0.05) **	0.06 (0.02) **
Liver	2.20 (0.50)**	1.39 (0.29)**	1.27 (0.72)**
Kidney	16.66 (5.78)	3.28 (0.82)**	3.34 (0.92)**
Small-intestine	0.53 (0.09)*	0.22 (0.05)**	0.29 (0.12)**
Large-intestine	0.40 (0.08)*	0.08 (0.01)**	0.33 (0.07)**
Spleen	1.86 (0.98)*	1.03 (0.35)**	0.89 (0.59)*
Pancreas	0.72 (0.12)**	0.15 (0.02)**	0.12 (0.07)*
Lung	5.86 (3.64)*	4.07 (2.99)*	2.49 (1.78)*
Heart	0.88 (0.18)*	0.24 (0.08)**	0.15 (0.07)**
Stomach[b]	0.36 (0.09)*	0.15 (0.12)	0.11 (0.04)**
Bone (Femur)	8.59 (0.55)**	11.81 (1.95)	12.88 (2.30)
Muscle	0.53 (0.11)	0.11 (0.07)	0.05 (0.02)
Brain	0.05 (0.01)	0.02 (0.00) *	0.01 (0.00)
F/B ratio[c]	4.50 (0.63)**	52.96 (17.28)**	229.73 (67.08)**

[a]Expressed as % injected dose. Each value represents the mean (SD) for five or six animals.
[b]Expressed as % injected dose.
[c]Femur:blood ratio.
*$p<0.05$ vs. control (no pretreatment).
**$p<0.01$ vs. control (no pretreatment).
doi:10.1371/journal.pone.0084335.t006

Table 7. Biodistribution of radioactivity after intravenous administration of ^{67}Ga-DOTA-Bn-SCN-HBP in mice with pretreatment of alendronate (20 mg/kg).[a]

	Time after administration		
Tissue	**10 min**	**1 h**	**3 h**
Blood	2.36 (0.20)**	0.87 (0.10)**	0.26 (0.05)**
Liver	1.59 (0.28)**	1.16 (0.21)**	0.54 (0.19)**
Kidney	13.84 (2.67)*	8.13 (1.39)**	6.42 (1.27)**
Small-intestine	0.61 (0.08)*	0.55 (0.07)**	0.38 (0.12)**
Large-intestine	0.37 (0.05)*	0.18 (0.01)**	0.38 (0.11)**
Spleen	1.42 (0.19)**	1.10 (0.25)**	0.69 (0.36)**
Pancreas	0.87 (0.15)**	0.36 (0.09)**	0.25 (0.06)**
Lung	3.06 (0.78)**	1.78 (0.18)**	0.57 (0.22) **
Heart	0.97 (0.22)*	0.43 (0.05)**	0.17 (0.05)*
Stomach[b]	0.47 (0.06)**	0.33 (0.05)**	0.23 (0.10)**
Bone (Femur)	8.59 (0.81)**	13.47 (1.76)**	13.30 (2.10)**
Muscle	0.57 (0.10)	0.35 (0.14)	0.19 (0.01)
Brain	0.06 (0.02)	0.04 (0.01)	0.02 (0.01)**
F/B ratio[c]	3.64 (0.20)**	15.82 (3.48)**	51.38 (5.91)**

[a]Expressed as % injected dose. Each value represents the mean (SD) for five or six animals.
[b]Expressed as % injected dose.
[c]Femur:blood ratio.
*$p<0.05$ vs. control (no pretreatment, Reference 29).
**$p<0.01$ vs. control (no pretreatment, Reference 29).
doi:10.1371/journal.pone.0084335.t007

(FITC)-labeled *N*-(2-hydroxypropyl)methacrylamide (HPMA) copolymers (P-ALN-FITC and P-D-Asp$_8$-FITC). In the study, P-D-Asp$_8$-FITC preferentially bound bone resorption surfaces, whereas P-ALN-FITC appeared to bind both formation and resorption surfaces in bone [46]. In hydroxyapatite binding experiments with different crystallinity, P-D-Asp$_8$-FITC showed preferential binding to hydroxyapatite of higher crystallinity compared with P-ALN-FITC. These observations indicated that bisphosphonate and aspartic acid peptides have different modes of hydroxyapatite binding. Accordingly, ^{68}Ga-DOTA-(Asp)$_{14}$ PET imaging may give different information than that obtained by ^{99m}Tc-MDP bone scintigraphy methods. Since ^{99m}Tc-MDP mainly accumulates osteoblastic lesions in bone, it has been known that sensitivity ^{99m}Tc-MDP often shows false-negative in osteolytic bone metastases lesions, and consequently, its sensitivity is reduced [47]. On the contrary, ^{68}Ga-DOTA-(Asp)$_{14}$ PET imaging may have a potential to improve its sensitivity. Meanwhile, in a previous ^{99m}Tc-MDP-bone scintigraphy study, treatments with bisphosphonate and alendronate may have caused false negative scintigraphy by producing competition between the drug and tracer, and blocking entrapment and accumulation of the tracer in bone [48]. In this study, pretreatment with alendronate inhibited bone accumulation of ^{67}Ga-DOTA-Bn-SCN-HBP more effectively than that of ^{67}Ga-DOTA-(Asp)$_{14}$, suggesting that bisphosphonate-induced false negative scintigraphy is less likely to occur in ^{68}Ga-DOTA-(Asp)$_{14}$ PET.

Radiogallium complexes of 1,4,7-triazacyclononane-triacetic acid (NOTA) or triazacyclononane-phosphinate (TRAP) may produce radiocomplexes with a higher specific activity than DOTA, allowing the use of much lower concentrations of precursor for labeling [49]. Despite this, DOTA was used in this study because unlike receptor imaging, much higher specific activity is not necessary for hydroxyapatite-targeted bone imaging. Moreover, DOTA is more versatile and could be developed for both imaging and therapeutics. Since the DOTA ligand forms a stable complex with not only gallium ($^{67/68}$Ga), but also lutetium (^{177}Lu) and yttrium (^{90}Y), which are beta particle emitters as radionuclides for therapy, furthermore, bismuth (^{213}Bi) as an alpha emitter could be applicable, its application to therapy from diagnosis could be made available. That is, radiometal complexes of DOTA-(Asp)$_n$ for radionuclide therapy could be useful as agents for the palliation of metastatic bone pain.

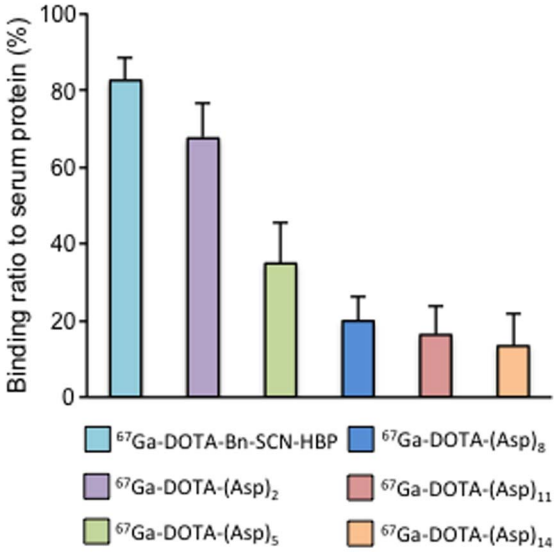

Figure 5. Serum protein binding. Serum protein binding ratios of ^{67}Ga-DOTA-(Asp)$_n$ (n = 2, 5, 8, 11, or 14) and ^{67}Ga-DOTA-Bn-SCN-HBP. Data are expressed as the mean ± SD for four samples.
doi:10.1371/journal.pone.0084335.g005

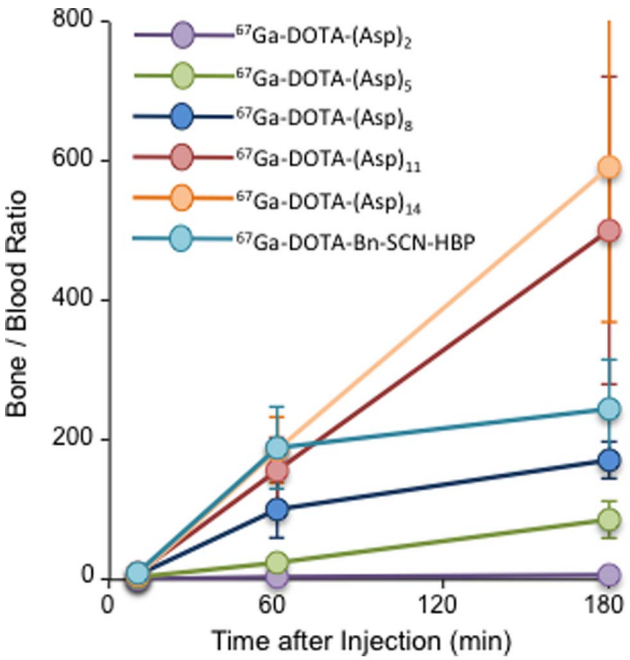

Figure 6. Bone/blood radio. Bone/blood ratio of radioactivity after injection of ^{67}Ga-DOTA-(Asp)$_n$ (n = 2, 5, 8, 11, or 14) and ^{67}Ga-DOTA-Bn-SCN-HBP. Data are expressed as the mean ± SD.
doi:10.1371/journal.pone.0084335.g006

In conclusion, the ^{67}Ga-DOTA complex-conjugated aspartic acid peptides ^{67}Ga-DOTA-$(Asp)_n$ showed ideal biodistribution characteristics as bone scintigraphy agents. Therefore, these agents may facilitate the drug design of PET tracers with ^{68}Ga for the diagnosis of bone disorders, such as bone metastases. Further studies are required to determine whether ^{68}Ga-DOTA-$(Asp)_n$ can provide additional information to that of bone scintigraphy, and to develop these compounds for radionuclide therapy.

Author Contributions

Conceived and designed the experiments: KO AO. Performed the experiments: KO AI KT. Analyzed the data: KO AI. Contributed reagents/materials/analysis tools: YK TK KS. Wrote the paper: KO.

References

1. Yoneda T, Sasaki A, Mundy GR (1994) Osteolytic bone metastasis in breast cancer. Breast Cancer Res Treat 32: 73–84.
2. Subramanian G, McAfee JG, Blair RJ, Kallfelz FA, Thomas FD (1975) Technetium-99m-methylene diphosphonate–a superior agent for skeletal imaging: comparison with other technetium complexes. J Nucl Med 16: 744–755.
3. Domstad PA, Coupal JJ, Kim EE, Blake JS, DeLand FH (1980) ^{99m}Tc-hydroxymethane diphosphonate: a new bone imaging agent with a low tin content. Radiology 136: 209–211.
4. Love C, Din AS, Tomas MB, Kalapparambath TP, Palestro CJ (2003) Radionuclide bone imaging: an illustrative review. Radiographics 23: 341–358.
5. Mari C, Catafau A, Carrio I (1999) Bone scintigraphy and metabolic disorders. Q J Nucl Med 43: 259–267.
6. Lavender JP, Khan RA, Hughes SP (1979) Blood flow and tracer uptake in normal and abnormal canine bone: comparisons with Sr-85 microspheres, Kr-81m, and Tc-99m MDP. J Nucl Med 20: 413–418.
7. Budd RS, Hodgson GS, Hare WS (1989) The relation of radionuclide uptake by bone to the rate of calcium mineralization. I: Experimental studies using ^{45}Ca, ^{32}P and ^{99}Tc^{m}-MDP. Br J Radiol 62: 314–317.
8. Budd RS, Hodgson GS, Hare WS (1989) The relation of radionuclide uptake by bone to the rate of calcium mineralization. II: Patient studies using ^{99}Tc^{m}-MDP. Br J Radiol 62: 318–320.
9. Galasko CS (1980) Mechanism of uptake of bone imaging isotopes by skeletal metastases. Clin Nucl Med 5: 565–568.
10. Libson K, Deutsch E, Barnett BL (1980) Structural characterization of a technetium-99-diphosphonate complex. Implications for the chemistry of technetium-99m skeletal imaging agents. J Am Chem Soc 102: 2476–2478.
11. Tanabe S, Zodda JP, Deutsch E, Heineman WR (1983) Effect of pH on the formation of Tc($NaBH_4$)-MDP radiopharmaceutical analogues. Int J Appl Radiat Isot 34: 1577–1584.
12. Ogawa K, Mukai T, Inoue Y, Ono M, Saji H (2006) Development of a novel ^{99m}Tc-chelate-conjugated bisphosphonate with high affinity for bone as a bone scintigraphic agent. J Nucl Med 47: 2042–2047.
13. Verbeke K, Rozenski J, Cleynhens B, Vanbilloen H, de Groot T, et al. (2002) Development of a conjugate of ^{99m}Tc-EC with aminomethylenediphosphonate in the search for a bone tracer with fast clearance from soft tissue. Bioconjug Chem 13: 16–22.
14. Palma E, Oliveira BL, Correia JD, Gano L, Maria L, et al. (2007) A new bisphosphonate-containing ^{99m}Tc(I) tricarbonyl complex potentially useful as bone-seeking agent: synthesis and biological evaluation. J Biol Inorg Chem 12: 667–679.
15. de Rosales RTM, Finucane C, Mather SJ, Blower PJ (2009) Bifunctional bisphosphonate complexes for the diagnosis and therapy of bone metastases. Chem Commun: 4847–4849.
16. Ogawa K, Mukai T, Arano Y, Hanaoka H, Hashimoto K, et al. (2004) Design of a radiopharmaceutical for the palliation of painful bone metastases: rhenium-186-labeled bisphosphonate derivative. J Labelled Cmp Radiopharm 47: 753–761.
17. Ogawa K, Mukai T, Arano Y, Otaka A, Ueda M, et al. (2006) Rhenium-186-monoaminemonoamidedithiol-conjugated bisphosphonate derivatives for bone pain palliation. Nucl Med Biol 33: 513–520.
18. Ogawa K, Mukai T, Arano Y, Ono M, Hanaoka H, et al. (2005) Development of a rhenium-186-labeled MAG3-conjugated bisphosphonate for the palliation of metastatic bone pain based on the concept of bifunctional radiopharmaceuticals. Bioconjug Chem 16: 751–757.
19. Ogawa K, Mukai T, Asano D, Kawashima H, Kinuya S, et al. (2007) Therapeutic effects of a ^{186}Re-complex-conjugated bisphosphonate for the palliation of metastatic bone pain in an animal model. J Nucl Med 48: 122–127.
20. Ogawa K, Mukai T, Kawai K, Takamura N, Hanaoka H, et al. (2009) Usefulness of competitive inhibitors of protein binding for improving the pharmacokinetics of ^{186}Re-MAG3-conjugated bisphosphonate (^{186}Re-MAG3-HBP), an agent for treatment of painful bone metastases. Eur J Nucl Med Mol Imaging 36: 115–121.
21. Uehara T, Jin ZL, Ogawa K, Akizawa H, Hashimoto K, et al. (2007) Assessment of ^{186}Re chelate-conjugated bisphosphonate for the development of new radiopharmaceuticals for bones. Nucl Med Biol 34: 79–87.
22. Torres Martin de Rosales R, Finucane C, Foster J, Mather SJ, Blower PJ (2010) ^{188}Re$(CO)_3$-dipicolylamine-alendronate: a new bisphosphonate conjugate for the radiotherapy of bone metastases. Bioconjug Chem 21: 811–815.
23. Ogawa K, Mukai T (2009) Targeted imaging and therapy for bone metastases: control of pharmacokinetics of bone-targeted radiopharmaceuticals. J Drug Deliv Sci Tec 19: 171–176.
24. Vitha T, Kubicek V, Hermann P, Elst LV, Muller RN, et al. (2008) Lanthanide(III) complexes of bis(phosphonate) monoamide analogues of DOTA: bone-seeking agents for imaging and therapy. J Med Chem 51: 677–683.
25. Ogawa K, Kawashima H, Shiba K, Washiyama K, Yoshimoto M, et al. (2009) Development of [^{90}Y]DOTA-conjugated bisphosphonate for treatment of painful bone metastases. Nucl Med Biol 36: 129–135.
26. Kubicek V, Rudovsky J, Kotek J, Hermann P, Vander Elst L, et al. (2005) A bisphosphonate monoamide analogue of DOTA: a potential agent for bone targeting. J Am Chem Soc 127: 16477–16485.
27. Blau M, Nagler W, Bender MA (1962) Fluorine-18: a new isotope for bone scanning. J Nucl Med 3: 332–334.
28. Even-Sapir E, Metser U, Mishani E, Lievshitz G, Lerman H, et al. (2006) The detection of bone metastases in patients with high-risk prostate cancer: 99mTc-MDP Planar bone scintigraphy, single- and multi-field-of-view SPECT, 18F-fluoride PET, and 18F-fluoride PET/CT. J Nucl Med 47: 287–297.
29. Zhernosekov KP, Filosofov DV, Baum RP, Aschoff P, Bihl H, et al. (2007) Processing of generator-produced ^{68}Ga for medical application. J Nucl Med 48: 1741–1748.
30. Notni J, Plutnar J, Wester HJ (2012) Bone-seeking TRAP conjugates: surprising observations and their implications on the development of gallium-68-labeled bisphosphonates. EJNMMI Res 2: 13.
31. Fellner M, Biesalski B, Bausbacher N, Kubicek V, Hermann P, et al. (2012) ^{68}Ga-BPAMD: PET-imaging of bone metastases with a generator based positron emitter. Nucl Med Biol 39: 993–999.
32. Suzuki K, Satake M, Suwada J, Oshikiri S, Ashino H, et al. (2011) Synthesis and evaluation of a novel ^{68}Ga-chelate-conjugated bisphosphonate as a bone-seeking agent for PET imaging. Nucl Med Biol 38: 1011–1018.
33. Ogawa K, Takai K, Kanbara H, Kiwada T, Kitamura Y, et al. (2011) Preparation and evaluation of a radiogallium complex-conjugated bisphosphonate as a bone scintigraphy agent. Nucl Med Biol 38: 631–636.
34. Fellner M, Baum RP, Kubicek V, Hermann P, Lukes I, et al. (2010) PET/CT imaging of osteoblastic bone metastases with ^{68}Ga-bisphosphonates: first human study. Eur J Nucl Med Mol Imaging 37: 834.
35. Butler WT (1989) The nature and significance of osteopontin. Connect Tissue Res 23: 123–136.
36. Oldberg A, Franzen A, Heinegard D (1988) The primary structure of a cell-binding bone sialoprotein. J Biol Chem 263: 19430–19432.
37. Oldberg A, Franzen A, Heinegard D (1986) Cloning and sequence analysis of rat bone sialoprotein (osteopontin) cDNA reveals an Arg-Gly-Asp cell-binding sequence. Proc Natl Acad Sci U S A 83: 8819–8823.
38. Kasugai S, Fujisawa R, Waki Y, Miyamoto K, Ohya K (2000) Selective drug delivery system to bone: small peptide $(Asp)_6$ conjugation. J Bone Miner Res 15: 936–943.
39. Yokogawa K, Miya K, Sekido T, Higashi Y, Nomura M, et al. (2001) Selective delivery of estradiol to bone by aspartic acid oligopeptide and its effects on ovariectomized mice. Endocrinology 142: 1228–1233.
40. Wang D, Miller S, Sima M, Kopeckova P, Kopecek J (2003) Synthesis and evaluation of water-soluble polymeric bone-targeted drug delivery systems. Bioconjug Chem 14: 853–859.
41. Kaiser E, Colescott RL, Bossinger CD, Cook PI (1970) Color test for detection of free terminal amino groups in the solid-phase synthesis of peptides. Anal Biochem 34: 595–598.
42. Ogawa K, Washiyama K (2012) Bone target radiotracers for palliative therapy of bone metastases. Curr Med Chem 19: 3290–3300.
43. Ogawa K, Saji H (2011) Advances in drug design of radiometal-based imaging agents for bone disorders. Int J Mol Imaging 2011: 537687.
44. Sekido T, Sakura N, Higashi Y, Miya K, Nitta Y, et al. (2001) Novel drug delivery system to bone using acidic oligopeptide: pharmacokinetic characteristics and pharmacological potential. J Drug Target 9: 111–121.
45. Meyer JL, Nancollas GH (1973) The influence of multidentate organic phosphonates on the crystal growth of hydroxyapatite. Calcif Tissue Res 13: 295–303.
46. Wang D, Miller SC, Shlyakhtenko LS, Portillo AM, Liu XM, et al. (2007) Osteotropic Peptide that differentiates functional domains of the skeleton. Bioconjug Chem 18: 1375–1378.

47. Kruger S, Buck AK, Mottaghy FM, Hasenkamp E, Pauls S, et al. (2009) Detection of bone metastases in patients with lung cancer: ^{99m}Tc-MDP planar bone scintigraphy, ^{18}F-fluoride PET or ^{18}F-FDG PET/CT. Eur J Nucl Med Mol Imaging 36: 1807–1812.
48. Demirkan B, Baskan Z, Alacacioglu A, Gorken IB, Bekis R, et al. (2005) False negative bone scintigraphy in a patient with primary breast cancer: a possible transient phenomenon of bisphosphonate (alendronate) treatment. Tumori 91: 77–80.
49. Notni J, Pohle K, Wester HJ (2012) Comparative gallium-68 labeling of TRAP-, NOTA-, and DOTA-peptides: practical consequences for the future of gallium-68-PET. EJNMMI Res 2: 28.